

Thomson backscattering in combined uniform magnetic and envelope modulating circularly-polarized laser fields

Julia Zhu^{1,*} and Bai-Song Xie^{2,3,†}

¹*Phillips Academy, Andover, MA 01810, USA*

²*College of Nuclear Science and Technology,
Beijing Normal University, Beijing 100875, China*

³*Beijing Radiation Center, Beijing 100875, China*

(Dated: March 4, 2022)

Abstract

The Thomson backscattering spectra in combined uniform magnetic and cosine-envelope circularly-polarized laser fields are studied in detail. With an introduction of the envelope modulation, the radiation spectra exhibit high complexity attributed to the strong nonlinear interactions. On the other hand, four fundamental laws related to the scale invariance of the radiation spectra are analytically revealed and numerically validated. They are the laws for the radiation energy as the 6th power of the motion constant exactly, also as the approximate negative 6th power with respect to the initial axial momentum and laser intensity in a certain of conditions, respectively, and finally an important self-similar law, i.e., when the circular laser frequency, the envelope modulation frequency, and the modified cyclotron frequency are simultaneously increased by a factor, the radiation energy will be increased by the second power of that factor without changing the shape of the spectrum. With the application of these laws, especially the last one, a much higher radiation energy can be obtained and the harmonic at which the maximum radiation occurs can be precisely tuned without changing its amplitude. These findings provide a possible way to advance radiation technology in many fields such as medicine, communications, astrophysics, and security.

PACS numbers: 41.60.-m, 52.59.-f, 89.75.Da

*Email: juliaz8888@gmail.com

†Corresponding author. Email: bsxie@bnu.edu.cn

I. INTRODUCTION

Due to its rich features and high potential of valuable applications in the radiation fields, scattering produced by electrons moving in laser fields has been studied extensively for almost half a century. As early as 1970, Sarachik and Schappert presented a classical theory of high-intensity Thomson scattering by an electron moving in an arbitrarily intense, elliptically polarized, plane electromagnetic field [1]; and, in 1993, Esarey *et al.* developed a comprehensive theory to describe the nonlinear Thomson scattering of intense laser field from beams and plasmas. They presented examples of possible laser synchrotron source configurations that are capable of generating hard and soft x-rays [2]. Salamin and Faisal further extended the study through their multiple publications on relativistic electron scattering in a superintense laser field [3–5]. In 2001, Umstadter examined the interactions between plasma electrons and laser light to produce compact laser radiation and caused more studies on improved energy spread [6]. Later, Lau *et al.*, in 2003, presented a classical analysis of Thomson scattering in an intense laser field and first introduced that the scattering spectra is dependent on the amplitude and phase of the electron motion [7]. He *et al.* also examined electrons accelerated by linearly polarized laser pulses and discovered the equation of the electron’s energy gain as a function of the electron’s initial position and scattering angle [8].

On the other hand, studies of a charged particle moving in an electromagnetic wave and a constant magnetic field, a setup of which is termed as ”autoresonance”, were pioneered by several researchers [9]. They found that the particle energy can increase indefinitely at certain conditions. In late 1990s and 2000, Salamin, Faisal, and Keitel presented the spectra of radiation emitted by an electron in a laser field and a uniform magnetic field [10–12]. Soon after, Yu *et al.* discovered that backscattered electrons can attain higher energies than forward-scattered electrons and analyzed the electron acceleration caused by linearly polarized laser pulses in a magnetic field and found that radiation occurs at high harmonics of the cyclotron frequency [13, 14]. In 2005, Gupta *et al.* analyzed electrons in combined oblique magnetic and circularly-polarized laser fields and found the optimal angle of the magnetic field for the highest energy [15]. In the following year Singh studied electrons accelerated by a circularly-polarized laser field in an axial magnetic field [16].

The autoresonance laser acceleration was further investigated over a wide range of laser

and magnetic field parameters by Galow *et al.* in 2013 [17]. They found that electron energy gains exceeding 100GeV are possible under certain conditions. In 2015, Salamin *et al.* [18] numerically investigated an electron vacuum autoresonance accelerator scheme which employs circularly polarized terahertz radiation and available magnetic fields and identified the parameters that could make the scheme experimentally feasible.

Recent studies of Thomson backscattering in combined uniform magnetic and polarized laser fields have been focused on the shape of the laser field. For example, in 2016, Fu *et al.* investigated it in the combined fields in which the laser field is circularly polarized [23]. Through numerical simulations, they found a scale invariance of the Thomson spectrum with respect to the laser intensity and initial axial momentum as scale factors in a high resonant regime [23], which can be as a natural but nontrivial extension of previous scaling law for the photon spectral density in [20] in the case of the presence of an external uniform magnetic field. Soon after, Jiang *et al.* extended the investigation to the combined fields with an elliptically-polarized laser field. The effects of the initial phase and ellipticity on the backscatter spectra and fundamental frequency were thoroughly analyzed [24].

Although the above publications found a scale invariance of the Thomson spectrum, mechanisms of increasing radiation strength and the tunability of the radiation source are still limited. In this study, we analytically prove and numerically validate that, if we introduce a cosine envelope to the circularly-polarized laser field combined with a uniform magnetic field, a high level of radiation strength and tunability can be obtained. As envisioned, once the cosine envelop is introduced, the radiation spectra exhibit very complicated phenomena. High oscillations appear in the radiation spectra, which are attributed to the strong nonlinear interactions with the interference effect of the electrons motion in the modulated laser pulse field [19, 21]. Obviously this enriches the optical-klystron-like phenomena reported in previous study [19] and the possible emitted spectral bandwidth controllability [21]. On the other hand, some simple smooth components of the radiation spectrum, named as ARS (Aggregated Radiation Spectra) curves, can be observed and extrapolated, which provides a convenient way to analyze the complicated radiation spectrum.

The advantage of envelop modulating laser field by a cosine enveloping function is that, obviously as an equivalent to the two-color field superposition, it is the highly nonlinear physical process for scattering spectra. Although simple two-color field addition due to the cosine-enveloped field, Thomson backscatter radiation does contain some basic yet very

important characteristics. In this study, we uncover and analytically prove four fundamental scaling laws related to the scale invariant of the radiation spectra. The first one states that, for an electron moving in combined uniform magnetic and cosine-enveloped circularly-polarized laser fields, the Thompson backscatter radiation energy is proportional to the 6th power of the motion constant. The second one states that the radiation spectrum shape is invariant with respect to the axial initial momentum of the electron. Moreover, when the axial initial momentum is much greater than 1, the radiation energy is proportional to the negative 6th power of the axial initial momentum. The third one states that, when the laser intensity and the resonant parameter are much greater than 1, the radiation energy is proportional to the negative 6th power of the laser intensity and the radiation spectrum shape is invariant with respect to the laser intensity. Lastly, the fourth one states that, when the circular frequency, the cosine-envelope frequency, and the modified cyclotron frequency are simultaneously increased by a factor of ρ , the Thomson backscatter radiation energy will be increased by a factor of ρ^2 without changing the shape of the spectrum.

The second and third laws are consistent to the numerical findings in the previous studies [23, 24], but the first and fourth laws are new in the present study. The significance of the fourth law can be highlighted by the following. First, the radiation energy can be greatly amplified with a simultaneous increase of the three frequencies of the envelope, the laser field and the cyclotron associated to the external applied uniform magnetic field strength. One example shows that the radiation intensity reaches 0.035, which is at a high strength we have never seen in all previous studies. Of course, the intensity can be tuned based on the needs by adjusting the scaling factor of these parameters. Second, the harmonic at which the maximum intensity occurs can be precisely tuned by adjusting the circular frequency relative to the enveloping one. This finding can greatly enhance the radiation technology in many fields, such as radiology, astrophysics, and communications.

One of the applications of this study is the production of THz emission. Based on their experiences with existing THz technology, a group of international THz science and technology experts from the fields of medicine, astrophysics, communications, and security repeatedly emphasized the need for tunable, high-power, yet low-cost THz emission [25]. For example, Wallace cited that the fields of dentistry and dermatology could be using THz radiation, but the cost of specialized lasers inhibits the wide purchase of such equipment [25]. With the usage of the cosine-envelope and the subsequent fourth law, high intensity

THz radiation can be emitted at a wide range of harmonics. This suggests that, with these findings, lower cost radiation set-ups can be more effective at producing intense radiation, potentially solving this cost dilemma for a variety of fields.

II. BASIC EQUATIONS

We consider the Thomson backscattering by an electron (with mass m and charge $-e$) moving in combined laser and magnetic fields. It is assumed that the laser field is a circularly-polarized plane wave with a modulated amplitude dependent upon a cosine function, vector potential amplitude A_0 , and laser frequency $\omega = \mu\omega_0$. Note that ω_0 is just a calibration frequency for the sake of convenience of normalization as below. The laser field propagates in the positive z direction, and the external uniform magnetic field B_0 is also assumed along the laser propagation direction. The phase unit of the laser field is denoted as $\eta = \omega_0\tau - \mathbf{k} \cdot \mathbf{R}$, where τ is time, \mathbf{k} is the laser wave vector, and \mathbf{R} is the electron displacement vector defined by $\mathbf{R} = X\hat{\mathbf{i}} + Y\hat{\mathbf{j}} + Z\hat{\mathbf{k}}$. The combinational total vector potential of fields can be expressed as

$$\mathbf{A} = A_0 \cos \alpha \eta (-\sin \mu \eta \hat{\mathbf{i}} + \cos \mu \eta \hat{\mathbf{j}}) + B_0 X \hat{\mathbf{j}}. \quad (1)$$

where μ represents the laser circular frequency coefficient and α represents the enveloping coefficient in a sense of calibration by ω_0 . When $\alpha = 0$, the laser field becomes a circularly-polarized plane wave with a constant amplitude (i.e. constant enveloping), which has been studied previously [23].

From the vector potential \mathbf{A} , the corresponding electric field \mathbf{E} and magnetic field \mathbf{B} are defined by the following equations:

$$\mathbf{E} = -\frac{1}{c} \frac{\partial \mathbf{A}}{\partial \tau}, \quad (2)$$

and

$$\mathbf{B} = \nabla \times \mathbf{A}. \quad (3)$$

The electron dynamics will be examined by applying the following momentum-energy evolving equations:

$$\frac{d\mathbf{P}}{d\tau} = -e(\mathbf{E} + \boldsymbol{\beta} \times \mathbf{B}), \quad (4)$$

and

$$\frac{d\gamma mc^2}{d\tau} = -ec\boldsymbol{\beta} \cdot \mathbf{E}, \quad (5)$$

where \mathbf{P} is the electron relativistic momentum, $\boldsymbol{\beta}$ is the electron velocity, and $\gamma = (1 - \beta^2)^{-\frac{1}{2}}$ is the electron relativistic factor. For convenience, we will normalize physical quantities with the following:

$$t = \omega_0 \tau, \quad z = kZ = \frac{\omega_0}{c} Z, \quad \mathbf{r} = \frac{\omega_0}{c} \mathbf{R}, \quad \boldsymbol{\beta} = \mathbf{v} = \frac{\mathbf{V}}{c}, \quad \mathbf{p} = \gamma \mathbf{v} = \frac{\mathbf{P}}{mc}.$$

Consequently, the phase of the laser field is now denoted as

$$\eta = t - z.$$

A. The Trajectory Solutions

From Eqs.(2) and (3), it can be proven that $E_x = B_y$ and $E_y = -B_x$, where the subscripts x and y respectively represent the x and y components of \mathbf{E} or \mathbf{B} . Applying these relationships to Eqs.(4) and (5) yields

$$\frac{dp_z}{d\tau} = -\frac{e}{mc} (\beta_x B_y - \beta_y B_x), \quad (6)$$

and

$$\frac{d\gamma mc^2}{d\tau} = mc^2 \frac{d\gamma}{d\tau} = -ec (\beta_x E_x + \beta_y E_y) = -ec (\beta_x B_y - \beta_y B_x). \quad (7)$$

Hence, $\frac{d\gamma}{d\tau} - \frac{dp_z}{d\tau} = 0$. Therefore, the constant of motion can be obtained as $\zeta = \gamma - p_z = \gamma_0 - p_{z0}$, although the electron moves in a varying-amplitude circularly-polarized laser field.

By substituting Eq.(1) into Eqs.(2) and (3), and further substituting the resulting expressions into Eq.(4), we obtain, after some manipulation, the motion equations of the electron:

$$\frac{d^2 p_x}{d\eta^2} + \omega_b^2 p_x = a \left((\omega_b + 2\mu) \alpha \sin \alpha \eta \cos \mu \eta + (\mu \omega_b + \alpha^2 + \mu^2) \cos \alpha \eta \sin \mu \eta \right) \quad (8)$$

$$\frac{d^2 p_y}{d\eta^2} + \omega_b^2 p_y = a \left((\omega_b + 2\mu) \alpha \sin \alpha \eta \sin \mu \eta - (\mu \omega_b + \alpha^2 + \mu^2) \cos \alpha \eta \cos \mu \eta \right) \quad (9)$$

where $a = \frac{eA_0}{mc^2}$ is the normalized laser intensity, $\omega_b = \frac{eB_0}{mc\zeta\omega_0}$ is the modified cyclotron frequency of the electron motion in the combined laser and magnetic fields.

Assuming that, at $t = 0$, $p_x = p_y = 0$, $p_z = p_{z0}$, and $\eta_{in} = z_{in}$, the momentum and energy of the electron can be determined from Eqs.(6), (7), (8), and(9):

$$p_x = an_1n_2 (c_1 \cos \omega_b \eta + c_2 \sin \omega_b \eta + q_{xp}) = an_1n_2 q_x \quad (10)$$

$$p_y = an_1n_2 (-c_2 \cos \omega_b \eta + c_1 \sin \omega_b \eta + q_{yp}) = an_1n_2 q_y \quad (11)$$

$$p_z = \frac{(an_1n_2)^2}{2\zeta} \left(c_1^2 + c_2^2 + m_1^2 \sin^2 \alpha \eta + m_2^2 \cos^2 \alpha \eta + 2(c_1 q_{xp} - c_2 q_{yp}) \cos \omega_b \eta \right. \\ \left. + 2(c_2 q_{xp} + c_1 q_{yp}) \sin \omega_b \eta \right) + \frac{1}{2\zeta} - \frac{\zeta}{2} \quad (12)$$

$$\gamma = \frac{(an_1n_2)^2}{2\zeta} \left(c_1^2 + c_2^2 + m_1^2 \sin^2 \alpha \eta + m_2^2 \cos^2 \alpha \eta + 2(c_1 q_{xp} - c_2 q_{yp}) \cos \omega_b \eta \right. \\ \left. + 2(c_2 q_{xp} + c_1 q_{yp}) \sin \omega_b \eta \right) + \frac{1}{2\zeta} + \frac{\zeta}{2}, \quad (13)$$

where

$$n_1 = \frac{1}{\omega_b - \alpha - \mu}, \quad n_2 = \frac{1}{\omega_b + \alpha - \mu},$$

$$c_1 = -q_{xp0} \cos \omega_b \eta_{in} - q_{yp0} \sin \omega_b \eta_{in},$$

$$c_2 = q_{yp0} \cos \omega_b \eta_{in} - q_{xp0} \sin \omega_b \eta_{in},$$

$$q_{xp} = m_1 \sin \alpha \eta \cos \mu \eta + m_2 \cos \alpha \eta \sin \mu \eta,$$

$$q_{yp} = m_1 \sin \alpha \eta \sin \mu \eta - m_2 \cos \alpha \eta \cos \mu \eta,$$

$$q_{xp0} = m_1 \sin \alpha \eta_{in} \cos \mu \eta_{in} + m_2 \cos \alpha \eta_{in} \sin \mu \eta_{in},$$

$$q_{yp0} = m_1 \sin \alpha \eta_{in} \sin \mu \eta_{in} - m_2 \cos \alpha \eta_{in} \cos \mu \eta_{in},$$

$$m_1 = \omega_b \alpha, \quad m_2 = \alpha^2 - \mu^2 + \omega_b \mu.$$

Unlike the constant enveloping laser field studied previously [23], the cosine-enveloped laser field which is equivalent to two-color field, combined with a uniform magnetic field would exhibit two singular points at $\omega_b = \alpha + \mu$ and at $\omega_b = -\alpha + \mu$. These two singular points correspond to the exact resonance condition of an electron in combined fields. For this reason, n_1 and n_2 represent the resonance parameters. Obviously, when ω_b is close to $\mu + \alpha$, then $n_1 \gg 1$; and when ω_b is close to $\mu - \alpha$, then $n_2 \gg 1$. Upon how close one can approach to resonance is that the cyclotron frequency by magnetic field approaches either

one of the two color fields. In fact, if there is no amplitude modulating field, the applied magnetic field is as high as $\sim (10^7\zeta - 10^8\zeta)$ Gauss for a typical laser field optical wavelength of $\lambda_L = 10\mu\text{m} - 1\mu\text{m}$, where ζ can reduce the magnetic field significantly if the electron is not at rest initially, for example, $B_0 \approx 5\text{MG}$ when $p_{z0} = 10$ for $\lambda_L = 1\mu\text{m}$. On the other hand, by introducing the cosine-function modulation, since $\mu - \alpha$ is usually smaller than μ , the applied magnetic field would be reduced further to some extent, when the resonance is approached. This is also one of the advantages of using a modulated laser field. Because under the exact resonance situations, in which either $1/n_1 = 0$ or $1/n_2 = 0$, the problem would be complex and have to be modified by the radiation damping force which can cause a certain of resonance width. In this paper, same as in previous publication [23] and others, we are not going to study the electron behaviors at the exact resonance cases. Rather, we will focus our study on the electron dynamics and related radiations that are close to or away from the resonance.

The trajectory equations of the electron are obtained via $\frac{dr}{d\eta} = \frac{p}{\zeta}$ as follows:

$$x(\eta) = \frac{an_1n_2}{\zeta} \left(\frac{1}{\alpha^2 - \mu^2} \left((-\alpha m_1 + \mu m_2) (\cos \alpha\eta \cos \mu\eta - \cos \alpha\eta_{in} \cos \mu\eta_{in}) \right. \right. \quad (14)$$

$$\left. \left. + (-\mu m_1 + \alpha m_2) (\sin \alpha\eta \sin \mu\eta - \sin \alpha\eta_{in} \sin \mu\eta_{in}) \right) + \frac{1}{\omega_b} \left(-c_2 (\cos \omega_b\eta - \cos \omega_b\eta_{in}) \right. \right.$$

$$\left. \left. + c_1 (\sin \omega_b\eta - \sin \omega_b\eta_{in}) \right) \right),$$

$$y(\eta) = \frac{an_1n_2}{\zeta} \left(\frac{1}{\alpha^2 - \mu^2} \left((\mu m_1 - \alpha m_2) (\sin \alpha\eta \cos \mu\eta - \sin \alpha\eta_{in} \cos \mu\eta_{in}) \right. \right. \quad (15)$$

$$\left. \left. - (\alpha m_1 - \mu m_2) (\cos \alpha\eta \sin \mu\eta - \cos \alpha\eta_{in} \sin \mu\eta_{in}) \right) + \frac{1}{\omega_b} \left(-c_1 (\cos \omega_b\eta - \cos \omega_b\eta_{in}) \right. \right.$$

$$\left. \left. + c_2 (-\sin \omega_b\eta + \sin \omega_b\eta_{in}) \right) \right),$$

$$\begin{aligned}
z(\eta) = & \frac{(an_1n_2)^2}{2\zeta^2} \left(c_1(m_1 + m_2) \frac{-\cos(\alpha + \mu - \omega_b)\eta + \cos(\alpha + \mu - \omega_b)\eta_{in}}{\alpha + \mu - \omega_b} \right. \\
& - c_1(m_1 - m_2) \frac{\cos(\alpha - \mu + \omega_b)\eta - \cos(\alpha - \mu + \omega_b)\eta_{in}}{\alpha - \mu + \omega_b} \\
& - c_2(m_1 - m_2) \frac{\sin(\alpha + \mu - \omega_b)\eta - \sin(\alpha + \mu - \omega_b)\eta_{in}}{\alpha + \mu - \omega_b} \\
& + c_2(m_1 + m_2) \frac{\sin(\alpha - \mu + \omega_b)\eta - \sin(\alpha - \mu + \omega_b)\eta_{in}}{\alpha - \mu + \omega_b} \\
& + \frac{1}{4} \left(2(m_1^2 + m_2^2)(\eta - \eta_{in}) + \frac{1}{\alpha}(m_1^2 - m_2^2)(-\sin 2\alpha\eta + \sin 2\alpha\eta_{in}) \right) \\
& \left. + (c_1^2 + c_2^2)(\eta - \eta_{in}) \right) + \frac{1 - \zeta^2}{2\zeta^2}(\eta - \eta_{in}). \tag{16}
\end{aligned}$$

In Eqs. (14) and (15), there seems to be a singular point at $\alpha = \mu$, but, when $\alpha = \mu$, $m_1 = m_2 = \omega_b$, allowing $\alpha - \mu$ to be canceled out from the denominators of both equations. Additionally, in Eq. (16), there seems to be a singular point at $\alpha = 0$. However, as α approaches 0, $\frac{1}{\alpha}(m_1^2 - m_2^2)(-\sin 2\alpha\eta + \sin \alpha\eta_{in})$ becomes $(m_1^2 - m_2^2)(-2\eta + 2\eta_{in})$. For this reason, we will separate our equations into two cases when necessary: for $\alpha = 0$ and for $\alpha \neq 0$.

It is observed from Eqs. (10-15) that the planar trajectory and momentum are periodic with a period of $T = 2\pi n$, where n is a smallest integer that makes each of the following terms an integer: $n\alpha$; $n\mu$; $n\omega_b$; $n(\omega_b - \alpha - \mu)$; $n(\omega_b + \alpha - \mu)$, which can be simplified as $n = \max(n_1, n_2)$ when the appropriate parameters are chosen to make either n_1/n_2 or n_2/n_1 an integer, see the Appendix A for details. Subsequently, $\mathbf{p}(\eta + T) = \mathbf{p}(\eta)$, $\mathbf{r}(\eta + T) = \mathbf{r}(\eta) + \mathbf{r}_0$, $\mathbf{r}_0 = (0, 0, z_0)$ where, for $\alpha \neq 0$,

$$z_0 = z(\eta + T) - z(\eta) = \frac{(an_1n_2)^2}{2\zeta^2} T \left(\frac{m_1^2 + m_2^2}{2} + c_1^2 + c_2^2 \right) + \frac{1 - \zeta^2}{2\zeta^2} T, \tag{17}$$

and for $\alpha = 0$

$$z_0 = z(\eta + T) - z(\eta) = \frac{(an_1n_2)^2}{2\zeta^2} T (m_2^2 + c_1^2 + c_2^2) + \frac{1 - \zeta^2}{2\zeta^2} T, \tag{18}$$

which represents the drift displacement of the electron during one period. Note that, for the case in which $\alpha = 0$ and $\mu = 1$, it can be proven that the trajectory, momentum, and energy equations are all recovered to the same equations as [23].

The above equations will be used to study the Thomson backscattering spectra in the following.

B. Emission Spectra

It is well known that the radiation energy emitted per unit solid angle $d\Omega$ and per unit frequency interval $d\omega$ is given by

$$\frac{d^2 I}{d\Omega d\omega} = \frac{e^2 \omega^2}{4\pi^2 c} |\mathbf{n} \times [\mathbf{n} \times \mathbf{F}(\omega)]|^2, \quad (19)$$

where the dimensionless form of vector $\mathbf{F}(\omega)$ is

$$\mathbf{F}(\omega) = \frac{1}{\zeta} \int_{-\infty}^{\infty} d\eta \mathbf{p}(\eta) \exp\left(i\omega(\eta - \mathbf{n} \cdot \mathbf{r}(\eta) + z(\eta))\right). \quad (20)$$

Since the electron is in a helical-type periodic motion, following the same approach as [23], the radiation energy can be decomposed into a radiation spectrum given by

$$\frac{d^2 I_m}{dt d\omega} = \frac{e^2}{4\pi^2 c} \frac{1}{\zeta^2} (m\omega_1)^2 (|\mathbf{F}_{mx}|^2 + |\mathbf{F}_{my}|^2), \quad (21)$$

where the m -th harmonic amplitude is now

$$\mathbf{F}_{mx,my} = \omega_1 a n_1 n_2 \int_{\eta_{in}}^{\eta_{in}+T} d\eta \mathbf{q}_{x,y}(\eta) \exp(im(\eta + 2z)\omega_1). \quad (22)$$

In the above equation ω_1 is the fundamental frequency of emitted harmonic spectra given by

$$\omega_1 = \frac{2\pi}{T - \mathbf{n} \cdot \mathbf{r}_0 + z_0}. \quad (23)$$

Note that for the case of Thomson backscatter, unit vector $\mathbf{n} = (0, 0, -1)$. Using Eqs. (17) or (18), ω_1 can be expressed as, for $\alpha \neq 0$,

$$\omega_1 = \frac{\zeta^2}{n + na^2(n_1 n_2)^2 \left(\frac{m_1^2 + m_2^2}{2} + c_1^2 + c_2^2 \right)}. \quad (24)$$

and, for $\alpha = 0$,

$$\omega_1 = \frac{\zeta^2}{n + na^2(n_1 n_2)^2 (m_2^2 + c_1^2 + c_2^2)}. \quad (25)$$

C. Fundamental Laws of Thomson Backscatter

In this section, we will reveal four fundamental scaling laws on the Thomson Backscatter of an electron moving in combined uniform magnetic and cosine-enveloped circularly-polarized laser fields.

For simplicity, we will assume $\eta_{in} = 0$ but keep in mind that all conclusions hold true for any η_{in} .

(1) Scaling law and scale invariant with respect to the motion constant of the electron: *For an electron moving in combined uniform magnetic and cosine-enveloped circularly-polarized laser fields, the Thomson backscatter radiation energy is proportional to the 6th power of the motion constant, and the radiation spectrum is invariant of the scaling induced by the motion constant.*

Since $\eta_{in} = 0$, we have

$$n_1 = \frac{1}{\omega_b - (\mu + \alpha)}, \quad n_2 = \frac{1}{\omega_b - (\mu - \alpha)}, \quad m_1 = \omega_b a, \quad m_2 = \alpha^2 - \mu^2 + \omega_b \mu, \quad c_1 = 0, \quad c_2 = -m_2,$$

$$q_x = -m_2 \sin \omega_b \eta + m_1 \sin \alpha \eta \cos \mu \eta + m_2 \cos \alpha \eta \sin \mu \eta, \quad (26)$$

$$q_y = m_2 \cos \omega_b \eta + m_1 \sin \alpha \eta \sin \mu \eta - m_2 \cos \alpha \eta \cos \mu \eta, \quad (27)$$

$$z = \frac{(an_1 n_2)^2}{2\zeta^2} \left(-m_2(\mu + \alpha) \sin \frac{\eta}{n_1} - m_2(\mu - \alpha) \sin \frac{\eta}{n_2} \right. \\ \left. + \frac{1}{4} \left(2(m_1^2 + m_2^2)\eta + \frac{1}{\alpha}(m_1^2 - m_2^2)(-\sin 2\alpha\eta) \right) + m_2^2 \eta \right) + \frac{1 - \zeta^2}{2\zeta^2} \eta, \quad (28)$$

and

$$\mathbf{F}_{mx,my} = \omega_1 a n_1 n_2 \int_0^T d\eta \mathbf{q}_{x,y}(\eta) \exp(im\omega_e(\eta)) \quad (29)$$

where $\omega_e(\eta)$ is an extended frequency defined by

$$\omega_e(\eta) = (\eta + 2z)\omega_1. \quad (30)$$

Substituting Eqs. (24) and (28) into Eq. (30), it gives

$$\omega_e(\eta) = \frac{(an_1 n_2)^2}{n + na^2(n_1 n_2)^2 \left(\frac{m_1^2 + m_2^2}{2} + m_2^2 \right)} \left(-m_2(\mu + \alpha) \sin \frac{\eta}{n_1} - m_2(\mu - \alpha) \sin \frac{\eta}{n_2} \right. \\ \left. + \frac{1}{4\alpha}(m_1^2 - m_2^2)(-\sin 2\alpha\eta) \right) + \frac{\eta}{n}. \quad (31)$$

It is evident that $\omega_e(\eta)$ does not explicitly contain the constant of motion. Moreover, neither $q_x(\eta)$ nor $q_y(\eta)$ contains ζ . The only term in Eq. (29) that has ζ is ω_1 (see Eq.(24)). Therefore, $\mathbf{F}_{mx,my}$ is linearly proportional to ζ^2 . From Eq. (21) it can be readily proven

that the radiation spectrum $\frac{d^2 I_m}{dt d\omega}$ is linearly proportional to ζ^6 . Since ζ is not present in the integrands of Eq. (29), the shape of the radiation spectrum is independent of the motion constant.

(2) Scaling law and scale invariant with respect to the axial initial momentum of the electron: *For an electron moving in combined uniform magnetic and cosine-enveloped circularly-polarized laser fields, the Thomson backscatter radiation spectrum shape is invariant with respect to the axial initial momentum of the electron. Moreover, when the axial initial momentum is much greater than 1, the radiation energy is proportional to the negative 6th power of the axial initial momentum.*

The invariant of the radiation spectrum with respect to p_{z0} is readily proven since it is not included in the integrands of Eq. (29). By definition, we have $\zeta = \sqrt{1 + p_{z0}^2} - p_{z0}$. For $p_{z0} \gg 1$, we have

$$\zeta \approx \frac{1}{2p_{z0}},$$

from which, we can conclude that the radiation spectrum $\frac{d^2 I_m}{dt d\omega}$ is linearly proportional to the negative 6th power of the initial axial momentum p_{z0} when p_{z0} is much greater than 1.

Note that the same law was numerically established in the previous study for the constant-enveloped laser field case [23].

(3) Scaling law and scale invariant with respect to the laser intensity: *For an electron moving in combined uniform magnetic and cosine-enveloped circularly-polarized laser fields, when the laser intensity and the resonant parameter are much greater than 1, the radiation energy is proportional to the negative 6th power of the laser intensity and the radiation spectrum shape is invariant with respect to the laser intensity.*

Under the condition of

$$a^2(n_1 n_2)^2 \left(\frac{m_1^2 + m_2^2}{2} + m_2^2 \right) \gg 1, \quad (32)$$

where it is easy to hold for high laser intensity and high resonant parameter. In this case, from Eq. (31) we have

$$\begin{aligned} \omega_e(\eta) = & \frac{1}{n \left(\frac{m_1^2 + m_2^2}{2} + m_2^2 \right)} \left(-m_2(\mu + \alpha) \sin \frac{\eta}{n_1} - m_2(\mu - \alpha) \sin \frac{\eta}{n_2} \right. \\ & \left. + \frac{1}{4\alpha} (m_1^2 - m_2^2)(-\sin 2\alpha\eta) \right) + \frac{\eta}{n}. \end{aligned}$$

Since neither q_x nor q_y contains a , the laser intensity a is no longer in the integrands of Eq. (29), which proves the scaling invariant with respect to a under the given condition of Eq. (32).

In addition, Eq. (29) now reads

$$\mathbf{F}_{mx,my} = \frac{\zeta^2}{ann_1n_2 \left(\frac{m_1^2+m_2^2}{2} + m_2^2 \right)} \int_0^T d\eta \mathbf{q}_{x,y}(\eta) \exp(im\omega_e(\eta)),$$

which indicates that $\mathbf{F}_{mx,my} \propto a^{-1}$.

Under the condition of Eq. (32), Eq(24) now simplifies to

$$\omega_1 = \frac{\zeta^2}{a^2n(n_1n_2)^2 \left(\frac{m_1^2+m_2^2}{2} + m_2^2 \right)},$$

it is seen that $\omega_1 \propto a^{-2}$. Using these proportions in Eq. (21), it is easy to check that $\frac{d^2I_m}{dt d\omega} \propto a^{-6}$.

Obviously this scaling law has also been numerically established in the previous study for the constant-enveloped laser field case [23].

(4) Scaling law and scale invariant with respect to the system's frequencies: *For an electron moving in combined uniform magnetic and cosine-enveloped circularly-polarized laser fields, when the circular frequency coefficient, the cosine-envelope frequency coefficient, and the modified cyclotron frequency are simultaneously increased by a factor of ρ , the Thomson backscatter radiation energy will be increased by a factor of ρ^2 without changing the shape of the spectrum.*

Assume that α , μ , and ω_b are changed by a factor of ρ as shown in the following

$$\alpha' = \rho\alpha, \quad \mu' = \rho\mu, \quad \omega'_b = \rho\omega_b.$$

Here we use ($'$) to represent a term after the change. In this case, we have

$$n'_1 = \frac{n_1}{\rho}, \quad n'_2 = \frac{n_2}{\rho}, \quad T' = \frac{T}{\rho}, \quad m'_1 = \rho^2 m_1, \quad m'_2 = \rho^2 m_2, \quad c_1 = 0, \quad c'_2 = \rho^2 c_2, \quad \omega'_1 = \rho\omega_1.$$

Substituting these expressions into Eqs. (26), (27), and (31) gives

$$\begin{aligned} q'_x &= \rho^2 q_x(\rho\eta), \\ q'_y &= \rho^2 q_y(\rho\eta), \\ \omega'_e(\eta) &= \omega_e(\rho\eta), \end{aligned}$$

and substituting the above equations into Eq. (29) yields

$$\mathbf{F}'_{mx,my} = \frac{\zeta^2 a n_1 n_2}{n + n a^2 (n_1 n_2)^2 \left(\frac{m_1^2 + m_2^2}{2} + m_2^2 \right)} \int_0^{\frac{T}{\rho}} d(\rho\eta) \mathbf{q}_{x,y}(\rho\eta) \exp(im\omega_e(\rho\eta)) = \mathbf{F}_{mx,my}.$$

Substituting the above equation into Eq. (21) proves that

$$\frac{d^2 I_m'}{dt d\omega} = \rho^2 \frac{d^2 I_m}{dt d\omega}. \quad (33)$$

The significance of this law will be discussed in the following section.

III. NUMERICAL RESULTS AND ANALYSIS

We first calculate the backscattering spectra of the m th order harmonic radiation with $p_{z0} = 0$, $a = 1$, $\alpha = 1$, $\mu = 7$, $\eta_{in} = 0$, and $\omega_b = 9$ by evaluating the spectra using harmonic m from 0 to 600 with an m -step size of 1. Note that the presented spectra intensity is normalized by $e^2/(4\pi^2 c)$, same as previous study [23]. The results are shown in Fig. 1(a). Evidently, as m varies, the backscattering radiation spectra oscillate drastically. However, Fig. 1(a) also exhibits types of continuous behaviors at a specific step size and initial value of harmonic m . For example, by utilizing a step size of m as 7 and an initial value of $m_{in} = 1$, (which means that we only plot the radiation spectrum at $m = 1, 8, 15, 22, \dots$), we are able to extrapolate a unique "smooth" curve, as shown in Fig. 1(b). Additional "smooth" curves can be obtained by varying the initial value of $m_{in} = 3$ and $m_{in} = 4$, as illustrated in Figs. 1(c) and 1(d). In this study, we name these "smooth" curves as the Aggregated Radiation Spectra curves (ARS curves). The main physical significance and conclusion is that the spectra are highly sensitive to the harmonics in some cases, which would be possible as an ultrashort THz source in the time domain.

To compare with the combined constant-enveloped laser field and a uniform magnetic field studied in [23], we calculate the spectra with $\alpha = 0$, $p_{z0} = 0$, $a = 1$, $\mu = 1$, $\eta_{in} = -2\pi \left(\left(\frac{na}{\zeta} \right)^2 + \frac{1}{2\zeta^2} - \frac{1}{2} \right)$, and $\omega_b = 1.1$ (which results in $n = 10$) by varying m from 0 to 2000 with a step size of 1. The results are shown in Fig. 2(a). Note that these results are consistent with [23]. We then calculate the spectra using the values of $\alpha = 0.1$ and $\omega_b = 1$ (which results in $n = 10$) while keeping all other parameters unchanged, shown in Fig. 2(b). Again, we find that high oscillations occur at lower harmonics until approximately $m = 600$. Two ARS curves can be extrapolated using even and odd harmonics. It is interesting to

see that the oscillations are constrained by these two ARS curves. Fig. 2(c) plots the curve with even harmonics, while Fig. 2(d) plots the curve with odd harmonics. Fig. 2(c) exhibits a higher peak at a higher harmonic than the peak in Fig. 2(d), but the graphs converge at around $m = 600$. If we closely examine Fig. 2(a), we can find that high oscillations do occur at very low-order harmonics. Therefore, it seems that both the constant-enveloped field and the cosine-enveloped field have high oscillations at very low harmonics, but solely in cosine-enveloped fields do high oscillations appear in a wide range of harmonics along with ARS curves.

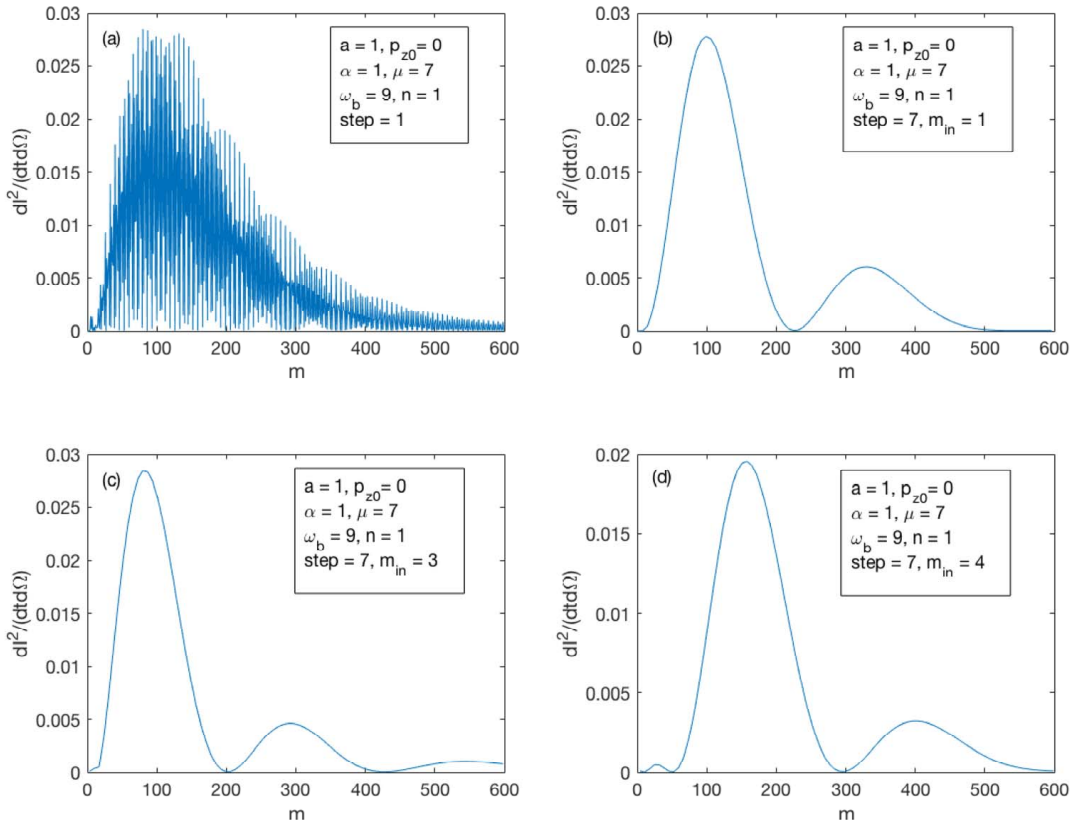


FIG. 1: The backscatter spectrum of m th-order harmonic radiation with different m_{in} and step sizes. (a): $a = 1$, $p_{z0} = 0$, $\alpha = 1$, $\mu = 7$, $\omega_b = 9$ plotting all integer values of m from 0 to 100. (b), (c) and (d): step size of m is set as 7, but with different $m_{in} = 1, 3$, and 4, respectively.

The physical explanation of the high oscillation phenomenon may be attributed to the highly nonlinear characteristics of the emitted spectra brought by the Thomson scattering process (see Eqs. (21) and (22)). The cosine-enveloping nature of the laser field further

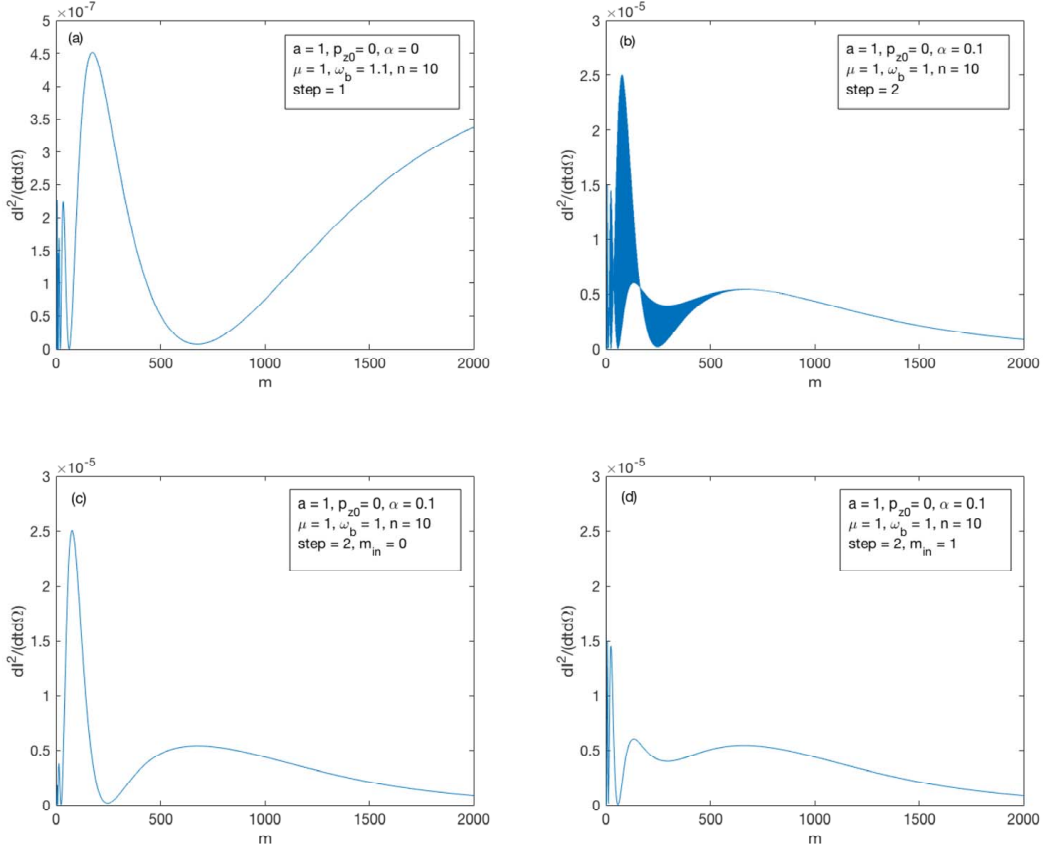


FIG. 2: The backscatter spectrum of m th-order harmonic radiation with different parameters. (a): $a = 1$, $p_{z0} = 0$, $\alpha = 0$, $\mu = 1$, $\omega_b = 1.1$, and $n = 10$. (b): Same as (a) except $\alpha = 0.1$ (ω_b adjusted accordingly). (c) and (d): Same as (b) except only even and odd harmonics are plotted, respectively.

enhances the nonlinear interactions, which leads to the interference effect of the electrons motion in modulated laser field.

Note that, in order to obtain the same resonant parameter $n = 10$, the modified cyclotron frequency ω_b needs to be 0.1 lower than in the constant enveloping case. Compared to Fig. 2(a), Fig. 2(b) shows that the peak amplitude is much higher but at a lower harmonic, which indicates that the cosine-envelope is capable of producing stronger radiation at a lower harmonic. Previous studies have proven that decreasing the laser intensity increases the Thomson backscatter radiation [23, 24]. In the case of the laser field discussed in this study, the cosine-envelope decreases the average laser field intensity, which, in turn, increases the backscattering. Therefore, besides causing high oscillations, the enveloped laser field is

also effective in producing high-energy backscatter radiation.

To further enforce the aforementioned conclusions, we study the case of $p_{z0} = 1$, $a = 0.5$, $\mu = 1$, $\eta_{in} = -2\pi \left(\left(\frac{na}{\zeta} \right)^2 + \frac{1}{2\zeta^2} - \frac{1}{2} \right)$, and $\omega_b = 1.2$ by varying the enveloping coefficient α to 0, 0.2, and 0.4. In order to maintain the same resonant parameter, $n = 5$, ω_b is modified accordingly. The results are plotted in Fig. 3. Again, we observe that Fig. 3(a) is consistent with [23], and high oscillations only occur at very low-order harmonics for both Figs. 3(a) and 3(b). Unlike Fig. 3(a), high-order harmonics dominate the spectrum in Fig. 3(b). Fig. 3(c) provides a closer look at the low-order harmonics of Fig. 3(b). As α increases, the high oscillations move into higher harmonic regions as shown in Fig. 3(d), and ARS curves can be clearly observed. As expected, the radiation amplitude increases significantly in the case of the enveloped laser field.

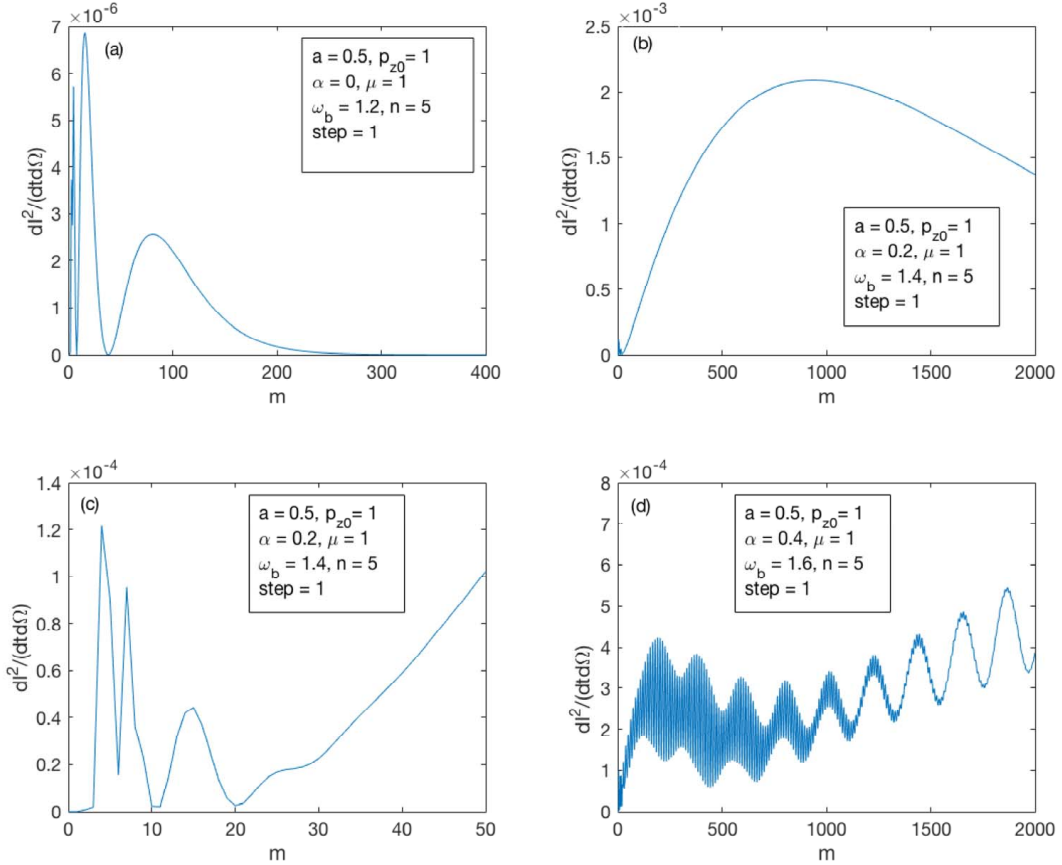


FIG. 3: The backscatter spectrum of m th-order harmonic radiation with different parameters. (a), (b), and (d): $a = 0.5$, $p_{z0} = 1$, $\mu = 1$, and $n = 5$ but $\alpha = 0$, 0.2, and 0.4 (ω_b adjusted accordingly), respectively. (c): Same as (b) except m is only plotted to 50.

In Figs. 4 and 5, we examine the effects of the laser field intensity a on the backscatter radiation with $\alpha = 0.1$, $\mu = 0.6$, and $\omega_b = 0.6$ ($n = 10$). For simplicity, we extrapolate an ARS curve using even harmonics. Figs. 4(a)-4(c) plot $a = 0.5$, $a = 1$, and $a = 2$, respectively, with $p_{z0} = 0$. It is apparent that, as the laser intensity a increases, the radiation intensity decreases, which is consistent with the scaling law of the laser intensity presented in the previous section. Since the a value is too small to satisfy Eq. (32), the shape of the curve does not remain unchanged. To satisfy Eq. (32), we increase a to 20 and 50, and the results are plotted in Figs. 5(a) and 5(b), respectively. Evidently, the shapes of the radiation spectra are almost the same in the two graphs, which numerically proves the scaling invariant law of the laser intensity.

The effects of the initial momentum p_{z0} are illustrated in Figs. 4(d)-4(f). Note that Fig. 4(d) is a repeat of Fig. 4(b) for clarity. From the figures, it is seen that, as p_{z0} increases, the amplitude of the spectrum decreases, but the shape of the radiation spectra remains unchanged. As expected, this result is consistent with the scaling law with respect to the motion constant and initial axial momentum.

Next, the effects of the circular frequency coefficient μ on the spectra are studied in Figs. 6(a) and 6(b), where $a = 1$, $p_{z0} = 0$, $\alpha = 0.1$, $n = 10$ (ω_b adjusted accordingly), $\eta_{in} = 0$, and $\mu = 0.5$ and 0.7 , respectively. It is observed that, as μ increases, the amplitude decreases and the peaks shift towards higher harmonics. This effect is further exhibited in Figs. 6(c) and 6(d) where α and μ and ω_b are all increased by a factor of ten.

Figs. 6(a) and 6(c) are an example of the fourth scaling law, which involves α , μ , and ω_b all increasing by a factor of 10 (n decreasing by the same factor). The scaling of these values results in a uniform magnification of the amplitude of the spectra by 10^2 . Figs. 6(c) and 6(d) demonstrate the same conclusion. Therefore, our fourth scaling law and scale invariance of the radiation spectrum is numerically justified.

The findings in Fig. 6 have at least two significance. First, the radiation energy can be greatly amplified with a simultaneous increase of α , μ , and ω_b . In our example, as shown in Fig. 6(c), the radiation intensity reaches 0.035, which is at a high strength we have never seen in all previous studies. Of course, the intensity can be tuned based on the needs by adjusting the scaling factor for α , μ , and ω_b . Second, the harmonic at which the maximum intensity occurs can be precisely tuned by adjusting the μ value relative to the α value. This can greatly enhance the radiation technology in many fields, such as radiology, astrophysics,

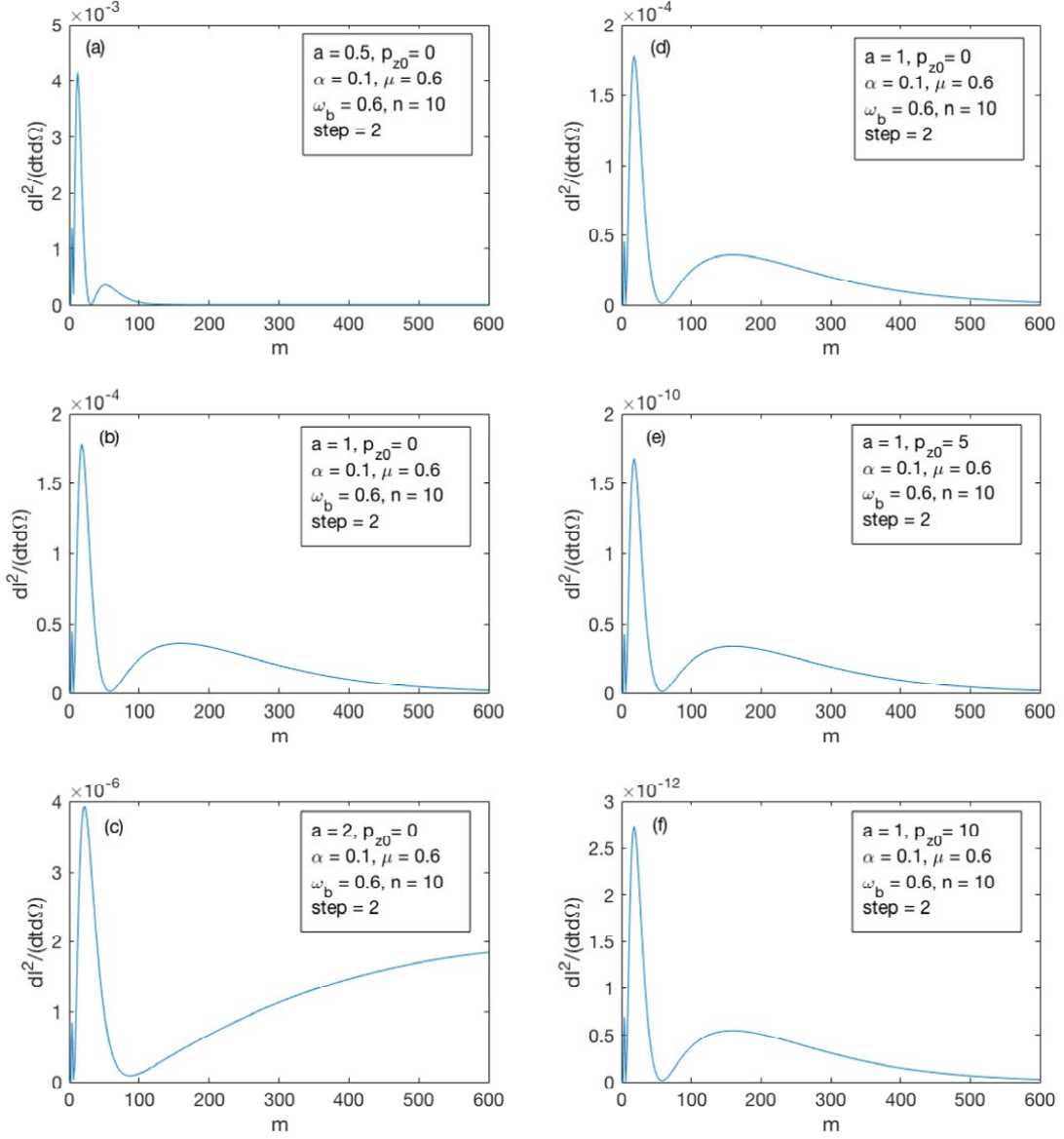


FIG. 4: The backscatter spectrum of m th-order harmonic radiation with different parameters. (a)-(c): $p_{z0} = 0$, $\alpha = 0.1$, $\mu = 0.6$, $\omega_b = 0.6$, $n = 10$, and $\text{step} = 2$, but $a = 0.5, 1$, and 2 , respectively. (d)-(f): $a = 1$, $\alpha = 0.1$, $\mu = 0.6$, $\omega_b = 0.6$, $n = 10$, and $\text{step} = 2$, but $p_{z0} = 0, 5$, and 10 , respectively.

and communications.

Because the cosine-enveloped laser field allows for two resonant parameters, in certain cases, there can exist two values of the modified cyclotron frequency ω_b for the same n value. Figs. 1(a) and 6(d) plot two different ω_b values with identical values for all other parameters. When comparing the two figures, it is seen that the larger ω_b produces higher peaks and more ARS curves and moves the peaks to higher harmonics. This suggests that, since ω_b is directly proportional to the magnetic field, a higher magnetic field can both increase the total energy as well as the complexity of the radiation spectrum.

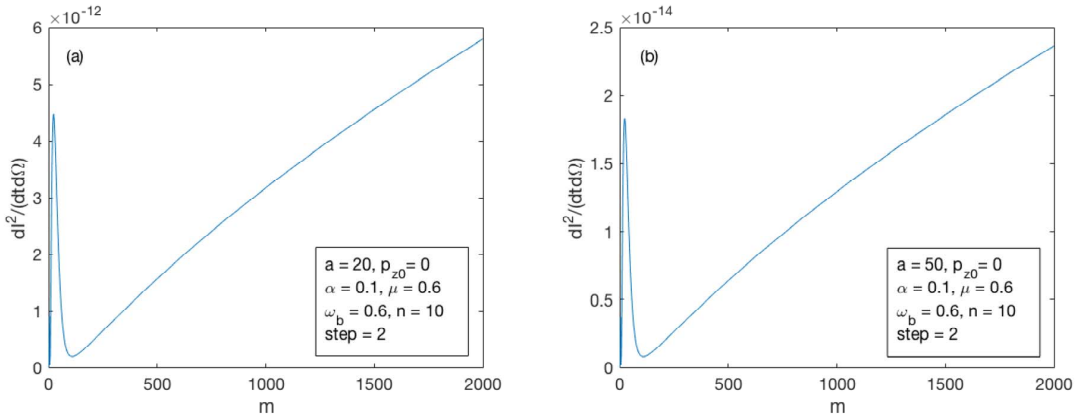


FIG. 5: The backscatter spectrum of m th-order harmonic radiation with different parameters. (a) and (b): $p_{z0} = 0$, $\alpha = 0.1$, $\mu = 0.6$, $\omega_b = 0.6$, $n = 10$, and $\text{step} = 2$, but $a = 20$ and 50 , respectively.

In Fig. 7, we further study the radiation spectra behavior under a high resonant parameter: when $n = 100$. A constant-enveloped laser field is compared to a slightly-enveloped laser field in Figs. 7(a) and 7(b), respectively. Once the cosine-envelope is introduced in Fig. 7(b), the peak amplitude increases, and the peak frequency moves to a lower harmonic. These behaviors are consistent with the conclusions of Figs. 2 and 3. On the other hand, since the enveloping coefficient α is very small in Fig. 7(b), the overall behavior is comparable to that of the constant envelope in Fig. 7(a). Unlike Figs. 2 and 3, however, we do not immediately observe drastic oscillations with the introduction of the cosine-envelope.

The absence of high oscillations in Fig. 7(b) deserves further analysis. We begin by gradually lowering the values of the laser intensity until $a = 0.55$, graphed in Fig. 7(c), at which high oscillations begin to form, indicating that $a = 0.55$ is a critical point. In

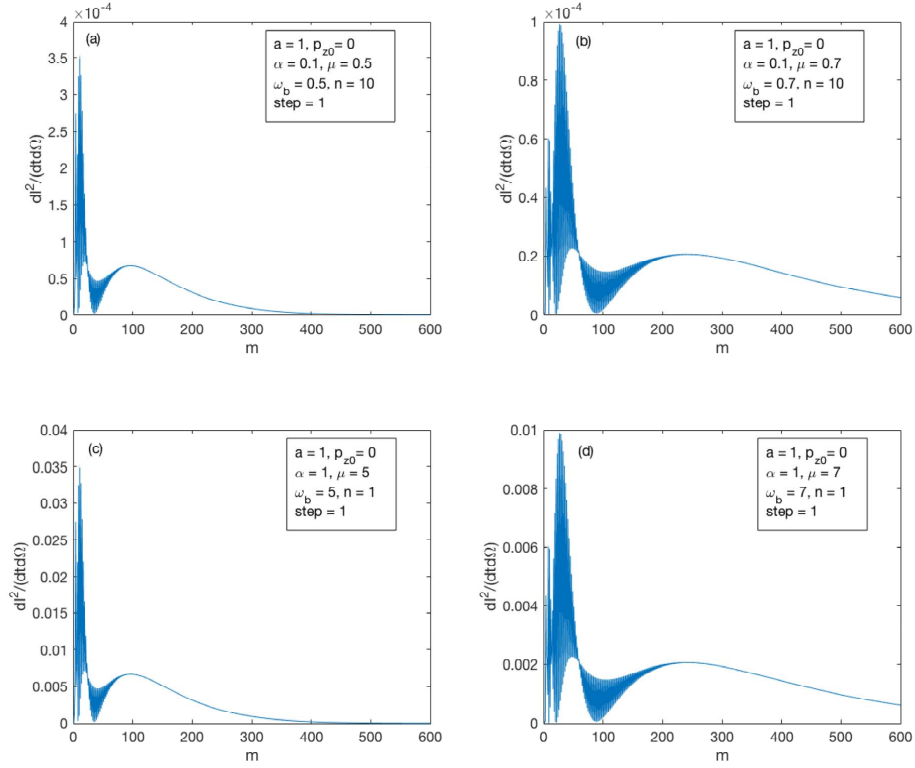


FIG. 6: The backscatter spectrum of m th-order harmonic radiation with different parameters. (a) and (b): $a = 1$, $p_{z0} = 0$, $\alpha = 0.1$, and $n = 10$, but $\mu = 0.5$ and 0.7 (ω_b changed accordingly), respectively. (c) and (d): Same as (a) and (b) except $\alpha = 1$ and $n = 1$, but $\mu = 5$ and 7 (ω_b changed accordingly), respectively.

addition, a strong ARS also forms, which gradually envelopes the high oscillation peaks. By further lowering a to 0.53 , the density of the high oscillations increases, and more ARS curves become noticeable with peaks slightly moving towards lower-harmonics. Further reductions of a to 0.52 and 0.5 exhibit the same overarching ARS curve, but clearer ARS curves with added complexity appear, resembling those of Fig. 1.

In the final examination of the numerical analysis, we apply the fourth scaling law to search for and produce high energy radiation in THz frequencies. Based on the experience from all the above numerical calculations and observations, we found that, at $a = 1$, $p_{z0} = 0$, $\alpha = 0.01$, $\mu = 0.05$, $\omega_b = 0.05$, and $n = 100$ and when the typical wavelength $\lambda = 1\mu m$ is used, a radiation intensity of about 3×10^{-6} can be obtained for harmonics $m = 1$ up to

$m = 9$, which corresponds to $0.3 - 3$ THz. These results are plotted in Fig. 8 where only odd harmonics are graphed for clarity. Note that the radiation intensity found here is 10^3 higher than what was obtained in [24]. Of course, optimal radiation is attainable through further tuning.

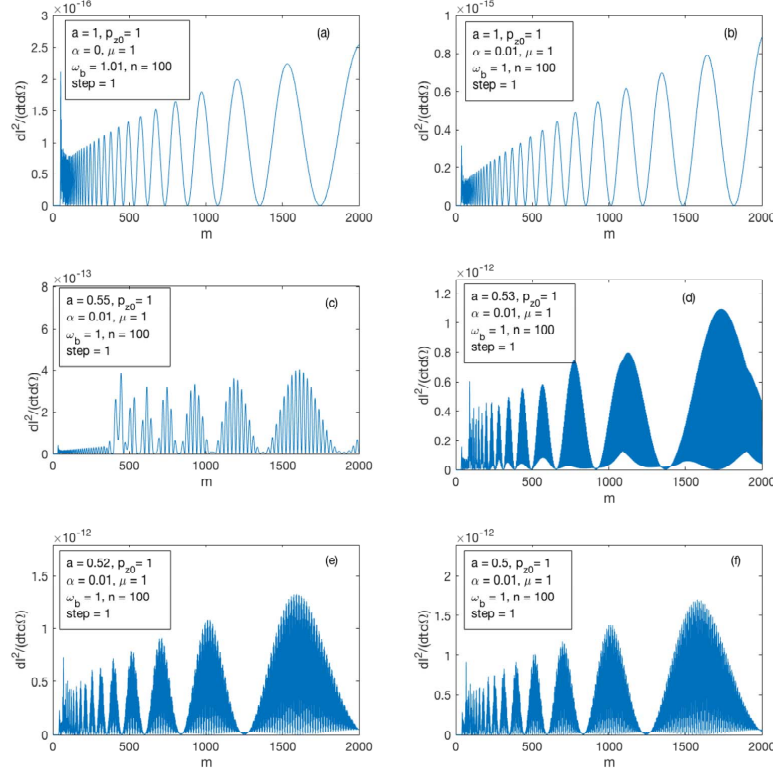


FIG. 7: The backscatter spectrum of m th-order harmonic radiation with different parameters. (a) $a = 1$, $p_{z0} = 1$, $\alpha = 0$, $\mu = 1$, $\omega_b = 1.01$, $n = 100$. (b): Same as (a) except $\alpha = 0.01$. (c)-(f): Same as (b) except $a = 0.55$, 0.53 , 0.52 , and 0.5 , respectively

In order to have a direct recognition of the intensity increased by our scheme presented here, we now compare some of the results in this paper to those in a well-known previous work [22]. As what He *et al.* have done, we denote the emission power in unit of erg/s as p_m (see Eq.(5) of [22]). Note that the normalizing intensity factor $e^2/4\pi^2c$ is 0.69 for $1\mu\text{m}$ laser wavelength. For simplicity, we can approximate it as ~ 1 . Two comparison examples will be given as the following. In the first example, we consider cases of Figs.2 (a) and 2(b), where the Thomson backscattering fundamental frequencies ω_1 correspond to $\sim 0.5\text{THz}$ and

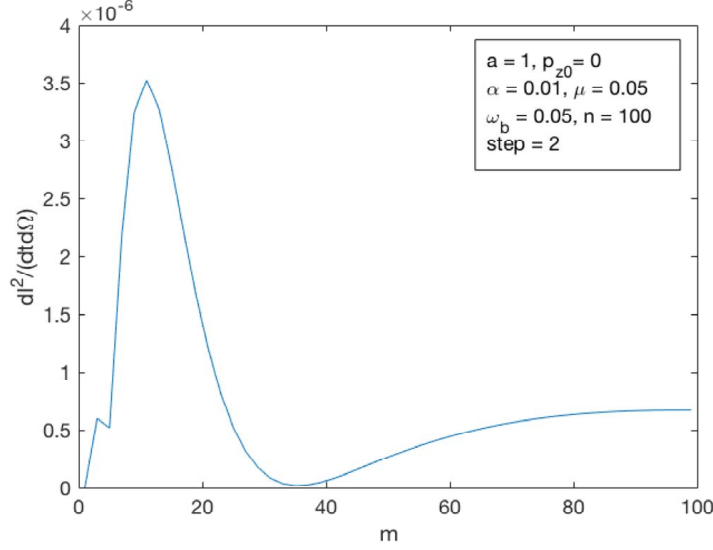


FIG. 8: The backscatter spectrum of m th-order harmonic radiation. $a = 1$, $p_{z0} = 0$, $\alpha = 0.01$, $\mu = 0.05$, $\omega_b = 0.05$, and $n = 100$. Odd harmonics are plotted from $m = 1$ to 100.

~ 2 THz. By matching these frequencies, the parameters of ζ of [22] (which can be denoted as ζ_{prl} in order to be distinguished from that of this paper) are $\zeta_{prl} \sim 0.03$ and $\zeta_{prl} \sim 0.06$. In this case, the corresponding emission powers in [22] are $\sim 10^{-9}$ and $\sim 10^{-8}$ in unit of erg/s. On the other hand, our results indicate that, when a magnetic field $\sim 10^8$ G is applied, the emission intensity is $\sim 10^{-7}$ in Fig.2(a) for $\alpha = 0$ and $\sim 10^{-5}$ in Fig.2(b) for $\alpha = 0.1$, which means that the presence of the magnetic field increases the intensity by 2 orders while the modulation of envelope further increases the intensity by another 2 orders. In the above example, our parameters correspond to the following system: laser intensity 10^{18} W/cm², wavelength $1\mu\text{m}$ (laser frequency $\sim 10^{15}$ Hz), magnetic field 10^8 G, and the initial electron rest energy ~ 0.5 MeV; and the corresponding parameters of [22] are the same except that there is no magnetic field and the initial electron energy is about $\sim (5 - 10)$ MeV. As the second example, we compare cases of Figs.3(a) and 3(b) to those in [22]. Now the fundamental frequency ω_1 is ~ 2.5 THz in Fig.3(a) and ~ 5 THz in Fig.3(b). In this case, the emission intensity is $\sim 10^{-6}$ in Fig.3(a) and $\sim 10^{-4}$ in Fig.3(b) which are 2 to 3 orders higher than what were obtained in [22]. The real physical parameters in this example are laser intensity $\sim 3 \times 10^{17}$ W/cm², wavelength $1\mu\text{m}$ (laser frequency $\sim 10^{15}$ Hz), magnetic field

$\sim 5 \times 10^7 \text{G}$, and the initial electron rest energy $\sim 0.5 \text{ MeV}$. The corresponding parameters in [22] are the same except that there is no magnetic field and the initial electrons energy is about $\sim (3 - 5) \text{ MeV}$. It is worthy to point out that the laser fields of [22] are linear but ours are circular. However, as shown in our previous work [24], the emission intensities of the linear field and the circular field are within the same order (only 2-3 times different). In addition, the laser intensity of linear to circular is about 2 times different. Therefore, the comparisons mentioned above are reasonable in the sense of magnitude orders.

IV. CONCLUSION AND DISCUSSION

In this paper, the Thomson backscattering spectra of an electron moving in the combined cosine-enveloped laser and magnetic fields have been studied. We have examined the effects of the cosine-envelope, the cyclotron frequency ω_b , the enveloping coefficient α , the circular frequency coefficient μ , the laser intensity a , the constant of motion ζ and the initial axial momentum p_{z0} on the radiation spectra.

As demonstrated in our numerical examples, with the introduction of the cosine-envelope, the radiation spectra exhibit complex and striking phenomenon. High oscillations appear in the radiation spectra, attributed to the strong nonlinear interactions. These oscillations can be further analyzed when extracted into ARS curves. We found that, for the same resonant parameter, a higher cyclotron frequency will produce more ARS curves and, similar to the effects of the enveloping coefficient, create an intense radiation spectra at higher harmonics. The circular frequency coefficient will shift the peaks of the radiation spectra to higher harmonics, but it has a negative correlation with the intensity of radiation spectra. Furthermore, the laser intensity, the constant of motion, and the initial axial momentum have an indirect correlation with the radiation spectra intensity as proven in three of the four major scaling laws of this study.

Analytically, we have derived and revealed four fundamental scaling laws for the case of the cosine-enveloped laser field that are upheld by the numerical results from this study. The scale invariance and scaling law of the constant of motion is described as $(d^2 I_m / dt d\omega) \propto \zeta^6$, and the scale invariance and scaling law of the enveloping coefficient, the circular frequency coefficient, and the modified cyclotron frequency is described as $(d^2 I_m / dt d\omega)' = \rho^2 (d^2 I_m / dt d\omega)$. Neither of these laws have been previously discovered in

other studies.

In particular, the fourth law is crucial to the amplification and tunability of the radiation spectra for further applications. In the plots given by this paper, by solely applying this law, radiation spectra intensities of 10^{-2} were obtained, which is remarkably higher than the intensities found in previous papers. In addition, radiation peaks can be intentionally tuned to both the right intensity and the right frequency.

Therefore it is expected to find that if one choose appropriately the laser and magnetic field parameters, the emitted spectral broaden width may be controlled and minimized, and the peak brightness of the emitted radiation can be increased by a existing scale factor of this study approximately. For example, in our last example case, we successfully applied the fourth fundamental law to produce high energy radiation in THz frequencies at an intensity of about 3×10^{-6} , which is 10^3 higher than what was obtained before [24]. The spectral bandwidth reduction of Thomson scattered light should be attributed the nonlinear interferences arising from the pulsed nature of the laser [21], which is also exhibited in our study here even if by using a simple cosine-envelope laser modulation. The findings in this research are believed to have a large potential to greatly enhance radiation technology for a number of applications from imagining to remote sensing to communications.

Acknowledgements

Much of the research was done by the first author under the mentorship of the second author. The first author is also grateful to C. Jiang, Z. Chen, and L. Zhao for some useful discussions. BSX is partially supported by the National Natural Science Foundation of China (NSFC) under Grant No. 11875007.

Appendix A: The determining of parameter n related to the period solution of electrons

From the solutions of electron about momenta and energy Eqs.(10-13), and also the positions Eqs(14-16), it is not difficult to see that there are three basic frequencies as

$$\Omega_1 = \mu + \alpha, \quad (\text{A1})$$

$$\Omega_2 = \mu - \alpha, \quad (\text{A2})$$

$$\Omega_3 = \omega_b, \quad (\text{A3})$$

and the three derivative difference frequencies among them as

$$\Omega_4 = \Omega_3 - \Omega_1 = \omega_b - (\mu + \alpha), \quad (\text{A4})$$

$$\Omega_5 = \Omega_3 - \Omega_2 = \omega_b - (\mu - \alpha), \quad (\text{A5})$$

$$\Omega_6 = \Omega_1 - \Omega_2 = 2\alpha. \quad (\text{A6})$$

Therefore there exists an integer n that satisfy the following algebraic equations, which make the solutions of momenta and positions are periodic except the net of displacement of z ,

$$n(\mu + \alpha) = l_1, \quad (\text{A7})$$

$$n(\mu - \alpha) = l_2, \quad (\text{A8})$$

$$n\omega_b = l_3, \quad (\text{A9})$$

$$(\text{A10})$$

where l_i ($i = 1, 2, 3$) are some integers. Obviously the $n\Omega_i = l_i$, where $i = 4, 5, 6$, are automatically satisfied.

Now for simplicity of numerical calculation and in fact without losing generality let us set $l_4 = 1$ or $l_5 = 1$. For the former case we have

$$n\Omega_4 = n/n_1 = l_3 - l_1 = 1, \quad (\text{A11})$$

$$n\Omega_5 = n/n_2 = l_3 - l_2, \quad (\text{A12})$$

$$n\Omega_6 = l_1 - l_2. \quad (\text{A13})$$

This means that the $n_1/n_2 = l$, where $l = l_3 - l_2$ is an integer of $|l| \geq 1$, the equality or inequality corresponds to the case of $\alpha = 0$ or $\alpha \neq 0$. So $n = n_1$ if we choose that

$$\omega_b = \mu + \alpha + \frac{\mu + \alpha}{l_3 - 1}$$

with some integer l_3 . It is equivalent to that if our choosing about ω_b making $n\omega_b$ is an integer then there must exist an integer l_3 satisfying the above equations. Once l_3 exists, the other required integer conditions of $l_1 = l_3 - 1, l_2 = l_3 - l, l_4 = 1, l_5 = l$ and $l_6 = l - 1$ are all satisfied automatically. In particularly the involved periodic requirement of emission power intensity appeared in Eq.(22) are that there exist at least one set of the relative-prime integers among $1, l, l - 1$. In fact there are two sets of relative-prime $1, l$ and $l, l - 1$ when $l = 2$, but complete three sets of relative-prime $1, l - 1, l$ when $l > 2$.

For the opposite case of $l_5 = 1$, where $n_2/n_1 = l$ is an integer of $|l| \geq 1$, the similar analysis mentioned above can be performed and now $n = n_2$. Therefore we have get the condition that the parameter n is determined by the combinational conditions of either n_1/n_2 or n_2/n_1 is an integer and $n = \max(n_1, n_2)$.

-
- [1] E. S. Sarachik and G. T. Schappert, Classical theory of the scattering of intense laser radiation by free electrons, Phys. Rev. D **1**, 2738 (1970).
 - [2] E. Esarey, S. K. Ride, and P. Sprangle, Nonlinear Thomson scattering of intense laser pulses from beams and plasmas, Phys. Rev. E **48**, 3003 (1993).
 - [3] Y. I. Salamin and F. H. M. Faisal, Harmonic generation by superintense light scattering from relativistic electrons, Phys. Rev. A **54**, 4383 (1996).
 - [4] Y. I. Salamin, Classical relativistic dynamics of a free electron in an intense laser field. Journal of Physics A: Mathematical and General **30**, 4399 (1997).
 - [5] Y. I. Salamin and F. H. M. Faisal, Harmonic generation by scattering circularly-polarized light of arbitrary intensity from free electrons of arbitrary initial velocity, Phys. Rev. A **55**, 3964 (1997).
 - [6] D. Umstadter, Review of physics and applications of relativistic plasmas driven by ultraintense lasers, Phys. of Plasmas **8**, 1774 (2001).
 - [7] Y. Y. Lau, Fei He, D. P. Umstadter, and R. Kowalczyk, Nonlinear thomson scattering: A tutorial, Phys. of Plasmas **10**, 2155 (2003).
 - [8] F. He, W. Yu, P. Lu, H. Xu, L. Qian, B. Shen, X. Yuan, R. Li, and Z. Xu, Ponderomotive acceleration of electrons by a tightly focused intense laser beam, Phys. Rev. E **68**, 046407 (2003).

- [9] A. A. Kolomenskii and A. N. Lebedev, Resonance effects associated with particle motion in a plane electromagnetic wave, *Sov. Phys. JETP* **17**, 179 (1963); C. S. Roberts and S. J. Buchsbaum, Motion of a charged particle in a constant magnetic field and a transverse electromagnetic wave propagating along the field, *Phys. Rev.* **135**, A381 (1964); V. S. Voronin and A. A. Kolomenskii, The pressure of an intense plane wave on a free charge and on a charge in a magnetic field, *Sov. Phys. JETP* **20**, 1027(1965); A. A. Kolomenskii and A. N. Lebedev, Quasilinear acceleration of particles by a transverse electromagnetic wave, *Sov. Phys. JETP* **23**, 733 (1966).
- [10] Y. I. Salamin and F. H. M. Faisal, Relativistic free-electron dynamics and lightemission spectra in the simultaneous presence of a superintense laser field and a strong uniform magnetic field, *Phys. Rev. A* **58**, 3221 (1998).
- [11] F. H. M. Faisal and Y. I. Salamin, Electron dynamics and photon-emission spectra in an ultrashort laser pulse and a uniform magnetic field, *Phys. Rev. A* **60**, 2505 (1999).
- [12] Y. I. Salamin, F. H. M. Faisal, and C. H. Keitel, Exact analysis of ultrahigh laser-induced acceleration of electrons by cyclotron autoresonance, *Phys. Rev. A* **62**, 053809 (2000).
- [13] W. Yu, V. Bychenkov, Y. Sentoku, M. Y. Yu, Z. M. Sheng, and K. Mima, Electron acceleration by a short relativistic laser pulse at the front of solid targets, *Phys. Rev. Lett.* **85**, 570 (2000).
- [14] W. Yu, Z. Y. Chen, M. Y. Yu, L. J. Qian, P. X. Lu, R. X. Li, and K. Koyama, Electron acceleration and high-order harmonic generation by an intense short pulse laser in a magnetic field, *Phys. Rev. E* **66**, 036406 (2002).
- [15] D. N. Gupta and C.-M. Ryu, Electron acceleration by a circularly-polarized laser pulse in the presence of an obliquely incident magnetic field in vacuum, *Physics of Plasmas*, **12**, 053103 (2005).
- [16] K. P. Singh, Acceleration of electrons by a circularly polarized laser pulse in the presence of an intense axial magnetic field in vacuum, *Journal of Applied Physics* **100**, 044907 (2006).
- [17] B. J. Galow, J. X. Li, Y. I. Salamin, Z. Harman, and C. H. Keitel, High-quality multi-GeV electron bunches via cyclotron autoresonance, *Phys. Rev. ST Accel. Beams* **16**, 081302 (2013).
- [18] Y. I. Salamin, J. X. Li, B. J. Galow, and C. H. Keitel, Feasibility of electron cyclotron autoresonance acceleration by a short terahertz pulse, *Optics Express* **23**, 17560 (2015).
- [19] C. A. Brau, Oscillations in the spectrum of nonlinear Thomson-backscattered radiation, *Phys. Rev. Accel. Beams* **7**, 020701 (2004).

- [20] D. Seipt and B. Kampfer, Scaling law for the photon spectral density in the nonlinear Thomson-Compton scattering, *Phys. Rev. Accel. Beams* **14**, 040704 (2011).
- [21] I. Ghebregziabher, B. A. Shadwick, and D. Umstadter, Spectral bandwidth reduction of Thomson scattered light by pulse chirping, *Phys. Rev. Accel. Beams* **16**, 030705 (2013).
- [22] F. He, Y. Y. Lau, D. P. Umstadter, and R. Kowalczyk, Backscattering of an intense laser beam by an electron, *Phys. Rev. Lett.* **90**, 055002 (2003).
- [23] Y. J. Fu, C. Jiang, C. Lv, F. Wan, H. B. Sang, and B. S. Xie, Scale invariance and scaling law of thomson backscatter spectra of electrons moving in the resonance regime in combined laser and magnetic fields, *Phys. Rev. A* **94**, 052102 (2016).
- [24] C. Jiang, H. Z. Xie, H. B. Sang, and B. S. Xie, Thomson backscattering in combined fields with a general elliptical polarization, *Europhysics Lett.* **117**, 44002 (2017).
- [25] S. S. Dhillon, M. S. Vitiello, E. H. Linfield, A. G. Davies, M. C. Hoffmann, J. Booske, C. Paoloni, M. Gensch, P. Weightman, G. P. Williams *et al.*, The 2017 terahertz science and technology roadmap, *Journal of Physics D: Applied Physics* **50**, 043001 (2017).
- [26] L. Zhao, Z. Chen, C. Jiang, J. Huang, C. Lv, B. S. Xie, and H. B. Sang, Angular distributions of Thomson scattering in combined laser and magnetic fields, *ArXiv: 1810.08333 v1* (2018).